Indonesian Journal of Electrical Engineering and Computer Science
Vol. 42, No. 3, June 2026, pp. 798~808
ISSN: 2502-4752, DOI: 10.11591/ijeecs.v42.i3.pp798-808

Optimization of glioma segmentation using 3D U-Net++ in MRI surgical planning and patient safety outcomes

Ahmed Bounegta, Mustapha Khelifi, Mohammed Beladgham
Laboratory of Information Processing and Telecommunication (LTIT), Department of Electrical Engineering, Faculty of Technology, University of TAHRI Mohammed, Bechar, Algeria

Article Info

Article history:

Received May 19, 2025
Revised Mar 31, 2026
Accepted May 26, 2026

Keywords:

3D convolution
Enhancing tumor
Glioma segmentation
MRI
Tumor core

ABSTRACT

The main goal of this study is to develop and evaluate a novel 3D U-Net++ convolutional neural network for accurate segmentation of glioma sub-regions in MRI scans, aiming to enhance surgical planning, targeted radiotherapy, and patient safety. Precise segmentation of glioma sub-regions is a persistent challenge in neuro-oncology due to substantial morphological variability across patients. To address this, we introduce an automatic segmentation model based on a 3D U-Net++ architecture with dense skip connections, which improves spatial feature extraction and the delineation of tumor boundaries. Utilizing volumetric data from the BraTS 2020 benchmark, the model automatically segments three clinically relevant substructures: tumor core, the enhancing tumor, and whole tumor. The integration of dense connections with 3D convolutional layers facilitates the detection of subtle tissue variations, including necrosis and edema. Quantitative evaluation demonstrates that the proposed 3D U-Net++ surpasses conventional architectures such as standard U-Net and DeepMedic in Dice coefficient, sensitivity, and specificity, yielding more homogeneous and continuous segmentations while reducing manual and semi-automatic annotation efforts. This approach supports advanced clinical decision-making and workflow automation, and offers potential for application to other tumor types or integration into real-time clinical practice.

Corresponding Author:

Ahmed Bounegta
Laboratory of Information Processing and Telecommunication (LTIT)
Department of Electrical Engineering, Faculty of Technology
University of TAHRI Mohammed
Bechar, Algeria
Email: bounegta.ahmed@univ-bechar.dz

1. INTRODUCTION

A large proportion of central nervous system cancers are gliomas, the most prevalent type of primary brain tumor [1], [2]. The precise segmentation of these tumors on MRI is essential for surgical planning, treatment, and patient follow-up [1], [3]. Doctors must carefully distinguish between the necrotic core, the enhanced tumor mass, and the edema, as this directly influences the prognosis and therapeutic options [2]-[6]. Currently, advanced 3D techniques are essential for effective planning [6]-[8], but manual and semi-automatic methods remain complex, time-consuming, and highly operator-dependent [8]-[10]. Automated 3D tumor segmentation from MRI has made significant progress thanks to the emergence of advanced deep learning architectures, improving the accuracy of glioma treatment. Menze *et al.* [1] established the BraTS challenge as a benchmark by providing multimodal databases that stimulated

algorithmic innovation. Building on these resources, Researcher [2], [8], then enriched them with expert radiomic annotations, offering more comprehensive datasets for model training and validation.

Initial models of 3D U-Net++ in articles by other authors [11], [12] have demonstrated exceptional performance. They leverage improved skip connections and dense feature propagation to achieve Dice coefficients that enhance whole tumor segmentation, with precision values slightly exceeding 0.99 on the BraTS2020 dataset. These architectures address the fundamental challenge of volumetric feature extraction while maintaining computational efficiency through optimized connection schemes. The 3D U-Net, developed by the authors of [13], was specifically designed to address dense volumetric segmentation from sparse annotations. This laid the groundwork for subsequent architectural improvements. Attention-based architectures also address tissue heterogeneity. Guan *et al.* [14] achieved Dice scores of 0.68 (whole tumor), 0.85 (tumor core), and 0.70 (enhancing tumor) on BraTS2020 by incorporating Squeeze-and-Excite filters and attention guidance mechanisms. BSAU-Net's [15] spatial and channel attention modules refined the boundaries, achieving a Dice score of >0.75 with a sensitivity of 0.90 and a precision of 0.78. The conclusions of articles [16]-[18] consistently rank the nnU-Net variants among the best. Implementations incorporating residual blocks, attention gates, and a Hausdorff distance loss yielded an average Dice of 0.83 and an HD95 of 3.8 mm for adult gliomas (Dice = 0.71, HD95 = 8.7 mm in pediatrics). Researcher [19], [20] for knowledge distillation in postoperative segmentation achieved a Dice of 0.836, highlighting its utility for surgical planning. External validations report a Dice of 0.81 to 0.86 across institutions. Ensemble and hybrid strategies enhance robustness. EnsembleUNets, combining several variants of U-Net, achieved a Dice score of 0.93 and HD95 of 18 mm on BraTS2021, surpassing CaPTk, 2DVNet, and ResNet50 [21], [22]. A 3D U-Net-LSTM fusion integrating temporal MRI patterns achieved an accuracy of 98.9%. The dual-modality sets achieved Dice = 0.9773 and average IoU = 0.6008.

Despite substantial progress in automated brain tumor segmentation, significant challenges remain in translating and generalizing these methods to clinical practice. Although state-of-the-art models achieve high Dice scores on curated datasets like BraTS, their performance often drops to 0.59–0.67 in real clinical settings. This decline in performance indicates a significant shift between the domains of training and deployment environments. Variations in acquisition parameters, scanner hardware, and imaging artifacts compromise the robustness of these systems. Delineating enhancing tumors is especially problematic: most methods achieve Dice scores of only 0.48 to 0.78 and show high Hausdorff distances without specialized loss functions, revealing persistent limitations in contour refinement. Postoperative and intraoperative segmentation are even more challenging due to brain movement, surgical artifacts, and strict real-time requirements. Finally, the lack of standardized evaluation metrics aligned with clinical needs perpetuates the gap between research benchmarks and practical utility, underscoring the need for models and protocols that can be reliably integrated into diverse clinical workflows.

This study examined a multi-objective loss function that combines weighted Dice, contour-sensitive Hausdorff, and focal modulation to balance overlap accuracy, contour fidelity, and class imbalance management. The function incorporates skip connections and integrates complex spatial data. On the BraTS2020 dataset, our optimized 3D U-Net++ model achieved a loss of 0.0146, an accuracy of 99.51%, a precision of 99.53%, and an average intersection over union (IoU) of 82.86%. This performance surpasses baseline U-Netmodels [13], [23] and DeepMedic models [3], [24]. Additionally, our model demonstrates superior boundary accuracy with Hausdorff distances lower than those of nnU-Net variants (approximately 3.8 mm). Model performance depends on architectural sophistication, loss function understanding, training data variety, and clinical evaluation metrics. The proposed loss function ensures high precision and low boundary error, both crucial for surgical planning and radiotherapy guidance.

2. WORK UNDERTAKEN and ENVIRONMENT

2.1. Summary of technical aspects

Integrating 3D U-Net++ architecture with advanced attention mechanisms and optimized skip connections significantly improves glioma segmentation accuracy and preoperative planning in MRI-guided neurosurgery [2], [13], [16], [25]. This framework enhances tumor margin delineation and enables consistent detection of intra-tumoral subregions, including necrotic cores and proliferative zones, essential for targeted therapeutic strategies [25]-[27]. Task-specific U-Net++ adaptations [11], [28] demonstrate computational efficiency and robustness in segmenting heterogeneous brain tumor subcomponents. This aligns with our study's objective to enhance medical imaging workflows through precise, automated segmentation protocols.

2.2. Work undertaken

This study illustrates that integrating intraoperative radiological monitoring (IRM) into preoperative glioma segmentation presents significant challenges due to tumor heterogeneity and irregularity in MRI data.

To address this, we apply a 3D U-Net++ model with dense skip connections and deep supervision to improve feature extraction and segment the enhancing tumor (ET), tumor core (TC), and peritumoral edema. Using the BraTS2020 dataset, we optimize performance with Dice Similarity Coefficient and 95th-percentile Hausdorff distance (HD95) metrics. This automated approach delivers accurate segmentation essential for neurosurgical planning, facilitates decision-making, and improves surgical outcomes.

This study addresses the challenges of glioma segmentation for preoperative planning, with a focus on intraoperative radiological monitoring. The proposed model utilizes a 3D U-Net++ architecture featuring dense skip connections and deep supervision to improve feature extraction and the segmentation of tumor subregions (see Table 1 for architectural details). A composite loss function is employed to capture structural features and reduce voxel-level misclassifications. The model's performance is evaluated on the BraTS2020 dataset, as illustrated in Figure 1, demonstrating its potential to enhance clinical decision-making and optimize surgical outcomes.

2.3. Environment: dataset & terms of use and description

2.3.1. Computational environment

All computational experiments were conducted on a high-performance PC equipped with an Intel Core i7 processor, 12 GB RAM, and Intel HD Graphics 3000 GPU, running a 64-bit operating system. For computationally intensive tasks, an NVIDIA Tesla P100 GPU available on Kaggle was utilized. The software environment comprised Python 3.8 and TensorFlow 2.4 to ensure robust machine learning performance.

2.3.2. Usage agreement

The BraTS-2020 datasets are freely available for research purposes, provided that appropriate acknowledgment is given by citing the main reference works. Specifically, users must cite the required manuscripts to comply with the dataset usage policy [1], [2], [29]. This ensures proper recognition of the original developers and upholds the integrity of academic research utilizing BraTS data.

2.3.3. Overview of the BraTS-2020 training dataset

The dataset contains MRI scans of high- and low-grade gliomas that were normalized, co-registered, and resampled for uniformity. Both high-grade and low-grade gliomas included annotated regions and clinical data. Tumor segmentation utilized four MRI modalities: T1, T1-Gd, T2, and FLAIR. Patient age and survival duration data support the development of prognostic models. The BraTS dataset comprises multimodal scans from 19 institutions, representing native T1, post-contrast T1-weighted (T1-Gd), T2-weighted, and T2-FLAIR volumes. BraTS2020 is particularly effective for brain tumor segmentation and survival prediction [29].

2.4. Methodological overview

The study employs a 3D U-Net++ model to segment gliomas in MRI volumes using 3D convolutions and dense skip connections for efficient multi-scale feature extraction [16], [30]. A progressive upsampling path refines spatial resolution to delineate necrotic/core, edema, and enhancing subregions [8], [31]. Using the BraTS2020 dataset, 100 slices per volume are selected, and performance is measured by Dice coefficient, accuracy, sensitivity, and specificity [10], [31]. The architecture's extensive skip pathways optimize feature reuse, lower memory requirements, and deliver a cost-effective, high-accuracy method for glioma segmentation [23], [31], supporting preoperative neurosurgical planning [2], [29]. Workflow stages include data preprocessing, model design [2], [13], loss function and metric selection, and ultimately, training with evaluation [18], [26].

2.5. Timeline of model implementations

The 3D U-Net++ model is categorized under the year 2018 in the image timeline shown in Figure 1. This year is characterized by improvements in sophisticated neural networks, particularly U-Net++, generative neural networks (GNNs), and DeepLab, which signify progress in intricate segmentation models for medical and scientific purposes. The 3D U-Net++ model, a variation of U-Net++, is an optimized architecture designed to improve feature extraction and segmentation precision in three-dimensional medical imaging.

The organization of this chart in Figure 1 comes after the first attempt at mathematical modeling of neurons in 1943 brought by McCulloch and Pitts, and the Perceptron in 1958, created by Frank Rosenblatt. This was one of the first binary classification algorithms.

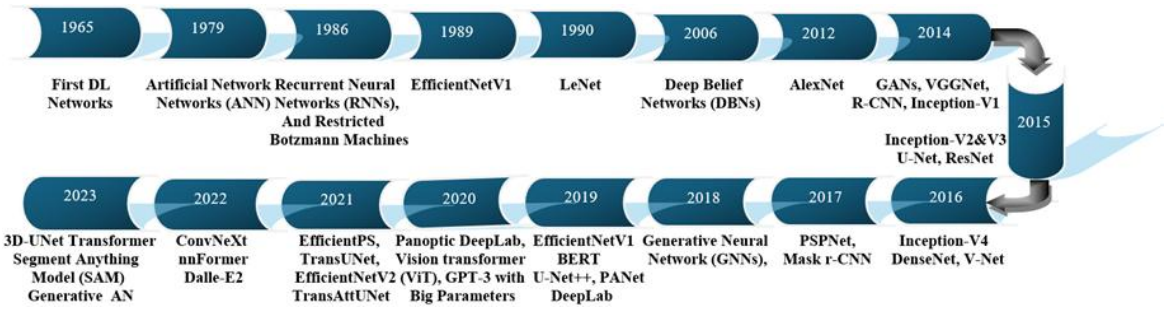

Figure 1. NET evolution chart (deep learning case)

3. NETWORK ARCHITECTURE

The composition and architecture dimensions of the implemented U-Net++ model used in this study are presented with detail in Table 1. This explanation highlights the network's structural design, including the representation of feature maps and the number of channels assigned to each layer, providing a comprehensive understanding of model's complexity. Special emphasis is placed on the 3D U-Net++ architecture, where each layer's role and connection are illustrated to reflect the advanced design of the executed model.

Table 1. The 3D U-Net++ architecture, with representation feature maps, and the number of channels is denoted for each layer (The executed model)

Layer (Type)	Output configuration	Param Number	Linked to
Input_layer_1 (Input layer)	(None, 128, 128, 128, 4)	0	-
conv3d (Conv3D)	(None, 128, 128, 128, 64)	6,976	input_layer_1[0][0]
conv3d_1 (Conv3D)	(None, 128, 128, 128, 64)	110,656	conv3d[0][0]
dropout (Dropout)	(None, 128, 128, 128, 64)	0	conv3d_1[0][0]
max_pooling3d (Max_Pooling3D)	(None, 64, 64, 64, 128)	0	dropout[0][0]
conv3d_2 (Conv3D)	(None, 64, 64, 64, 128)	221,312	max_pooling3d[0][0]
conv3d_3 (Conv3D)	(None, 64, 64, 64, 128)	442,496	conv3d_2[0][0]
dropout_1 (Dropout)	(None, 64, 64, 64, 128)	0	conv3d_3[0][0]
Max_pooling3d_1 (Max_Pooling3D)	(None, 32, 32, 32, 128)	0	dropout_1[0][0]
conv3d_4 (Conv3D)	(None, 32, 32, 32, 2)	884,992	max_pooling3d_1[0][0]
conv3d_5 (Conv3D)	(None, 32, 32, 32, 2)	1,769,728	conv3d_4[0][0]
dropout_2 (Dropout)	(None, 32, 32, 32, 2)	0	conv3d_5[0][0]
max_pooling3d_2 (MaxPooling3D)	(None, 16, 16, 16, 2)	0	dropout_2[0][0]
conv3d_6 (Conv3D)	(None, 16, 16, 16, 5)	3,539,456	max_pooling3d_2[0][0]
conv3d_7 (Conv3D)	(None, 16, 16, 16, 5)	7,078,400	conv3d_6[0][0]
dropout_3 (Dropout)	(None, 16, 16, 16, 5)	0	conv3d_7[0][0]
max_pooling3d_3 (MaxPooling3D)	(None, 8, 8, 8, 512)	0	dropout_3[0][0]
conv3d_8 (Conv3D)	(None, 8, 8, 8, 1024)	14,156,800	max_pooling3d_3[0][0]
conv3d_9 (Conv3D)	(None, 8, 8, 8, 1024)	28,312,576	conv3d_8[0][0]
dropout_4 (Dropout)	(None, 8, 8, 8, 1024)	0	conv3d_9[0][0]
up_sampling3d (UpSampling3D)	(None, 16, 16, 16, 1)	0	dropout_4[0][0]
conv3d_10 (Conv3D)	(None, 16, 16, 16, 5)	14,156,288	up_sampling3d[0][0]
Concatenate (Concatenate)	(None, 16, 16, 16, 1)	0	dropout_3[0][0]/conv3d_10[0][0]
conv3d_11 (Conv3D)	(None, 16, 16, 16, 5)	14,156,288	concatenate [0][0]
concatenate (Concatenate)	(None, 16, 16, 16, 1024)	0	dropout_3[0][0]/ conv3d_10[0][0]
Conv3d_11 (Conv3D)	(None, 16, 16, 16, 256)	14,156,288	concatenate [0][0]
up_sampling3d_3 (UpSampling3D)	(None, 128, 128, 128, 128)	0	dropout_7[0][0]
Conv3d_16 (Conv3D)	(None, 128, 128, 128, 64)	221,248	up_sampling3d_3[0][0]
dropout_8 (Dropout)	(None, 128, 128, 128, 64)	0	conv3d_17[0][0]
conv3d_16 (Conv3D)	(None, 128, 128, 128, 4)	260	dropout_[0][0]

Total parameters: 94,126,852 (359.07 MB), Trainable params: 94,126,852 (359.07 MB)

4. EXECUTION AND SPECIFICATIONS

4.1. Information

The 3D U-Net++ model for brain tumor segmentation has two primary components: data preparation and training configuration. Data preparation entails importing 3D MRI volumes, normalizing voxel intensities, employing augmentation techniques, and delineating segmentation masks for tumor subregions. Batch production involves partitioning the dataset into training, validation, and test subsets: 68% for training, 20% for validation, and 12% for testing. The training dataset was internally split for validation, using 85% for training and 15% for testing during the training phase.

4.2. Equations and mathematical formulations

4.2.1. Importance in image segmentation

In segmentation, the Dice coefficient indicates how much the segmented area in the prediction overlaps with the ground truth. A higher Dice coefficient indicates a better performance.

4.2.2. Mathematical formulation

- The Dice coefficient (F1-score)

D between two sets A and B (representing the predicted segmentation and the ground truth, re-spectively) is formulated as:

$$D = \frac{2|A \cap B|}{|A|+|B|} \quad (1)$$

Where:

- |A∩B| is the intersection (overlap) between the predicted and true sets,
- |A| and |B| are the sizes (pixel counts) of the respective sets.
- In segmentation (classification) tasks, such as tumor border identification, HD5 is essential as it prevents slight mistakes at distant places from significantly distorting the distance metric, result-ing in a more dependable assessment of spatial closeness.

Mathematically, HD95 calculates the Hausdorff distance at the 95th percentile, formulated as follows:

$$HD95(A,B) = max\left(percentile_{95}\left(\begin{matrix}min\\ b\in B\end{matrix} d(a,b)\right),\ \ percentile_{95}\left(\begin{matrix}min\\ a\in A\end{matrix} d(a,b)\right)\right) \quad (2)$$

where: d(a, b) represents the Euclidean distance be-tween points a∈A and b∈B.

- Sensitivity, or true positive rate, is vital in healthcare for the precise identification of positive cases, reducing false negatives, and is fundamental for classification jobs.
- Sensitivity is defined as:

$$S = \frac{True\ Positives\ (TP)}{True\ Positives\ (TP)+False\ Negatives\ (FN)} \quad (3)$$

where:

- True positives (TP) are correctly identified positive instances,
- False negatives (FN) are positive instances incorrectly identified as negative.
- Specificity (T), or true negative rate, is an essential statistic in fraud detection, facilitating the precise identification of negative cases and minimizing false positives, especially in screening tests.

$$S' = \frac{True\ Negatives\ (TN)}{True\ Negatives\ (TN)+False\ Positives\ (FP)} \quad (4)$$

Where:

- True negatives (TN) are correctly identified negative instances,
- False positives (FP) are negative instances incorrectly identified as positive.
- Dice loss is a mathematical formula that optimizes the Dice coefficient in segmentation tasks by penalizing models for low overlap between predicted and ground truth segments.

Dice loss:

$$L_{Dice} = 1 - \frac{2|A \cap B|}{|A|+|B|} \quad (5)$$

where: The notation is similar to the Dice coefficient but optimized for gradient-based learning.

4.3. Instruction

The 3D U-Net++ model employs dense skip connections, composite loss functions, callbacks, and regularization to enhance segmentation accuracy and generalization. Evaluated on a test set, it ensures precise delineation of tumor subregions while maintaining spatial and contextual integrity. Vertical skip connections and 3D convolutions facilitate effective information flow and volumetric feature retention, making the architecture well-suited for accurate brain tumor segmentation.

5. COMPUTING EXPERIMENTS

This research focuses on the specific methodology for completely automated segmentation studies of brain tumors using the U-Net++ 3D model. The process follows:

Data Preparation and Training Configuration for MRI Segmentation Utilizing 3D U-Net++: MRI volumes are preprocessed, and user-provided annotations mark initial tumor regions to guide segmentation. Data augmentation techniques like rotation and scaling expand dataset diversity while preserving annotation accuracy. A 3D U-Net++ model with skip connections is trained using Dice and cross-entropy losses to boost segmentation performance and minimize overfitting. User feedback via callbacks allows refinement of complex slices, further improving model accuracy, which is assessed using Dice, sensitivity, and precision metrics to highlight the benefits of semi-automation in marked areas.

Visualization tools display MRI data used for deep learning-based brain tumor segmentation, aiding precise tumor boundary identification and preoperative planning for individual patients. The code retrieves multiple MRI modalities (FLAIR, T1, T1ce, T2) scans, along with a ground truth segmentation mask for a single patient in Figure 2, case (BraTS20_Training_001). Using the NiBabel library, the code reads each MRI scan in. nii format and extracts its data as a 3D numpy array.

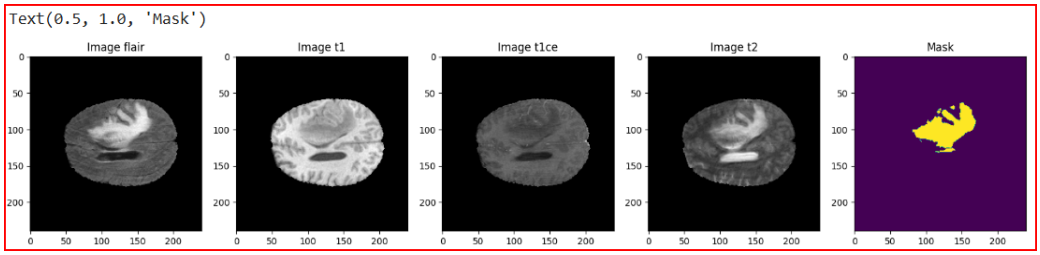

Figure 2. Illustration of different MRI modalities for a single patient case (BraTS20_Training_001)

5.1. For further analysis of the resulting images, of the simulated code sequence

The Animated Visualization presented in Figures 3 and 4 illustrates MRI data employed for training deep learning models in brain tumor segmentation. This dynamic, layer-by-layer GIF vividly showcases the three-dimensional spatial relationships among anatomical structures, offering an intuitive understanding of complex brain morphology. By enhancing the visibility of tumor boundaries and adjacent tissues, the visualization significantly contributes to improving segmentation accuracy and supports more effective pre-operative planning and clinical decision-making.

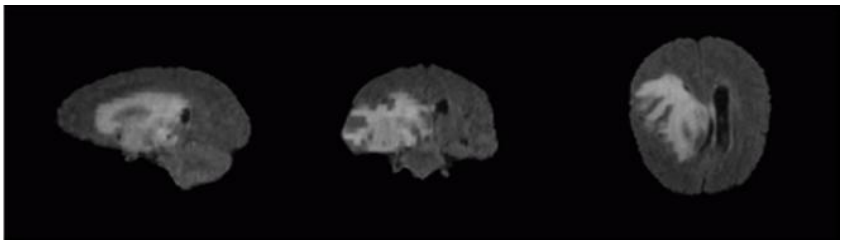

Figure 3. Interactive representation of cross-sections in a 3D volume (GIF)

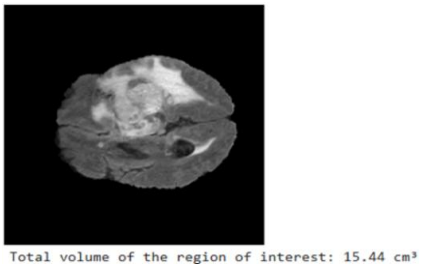

Figure 4. Brain_volume.gif' for the first slice (001)

The following graphic shows Plot_roi visualization, which helps researchers understand brain scan representations that highlight the presence of tumors (Figure 5), check segmentation accuracy, and refine models for better clinical outcomes.

The model's training history was used to evaluate its segmentation performance, identify trends, and assess stability. Key indicators were examined to understand the adaptation of the model during training. The model's behavior was compared on training and validation datasets to ensure its generalizability for new and unpublished data, in Figure 6.

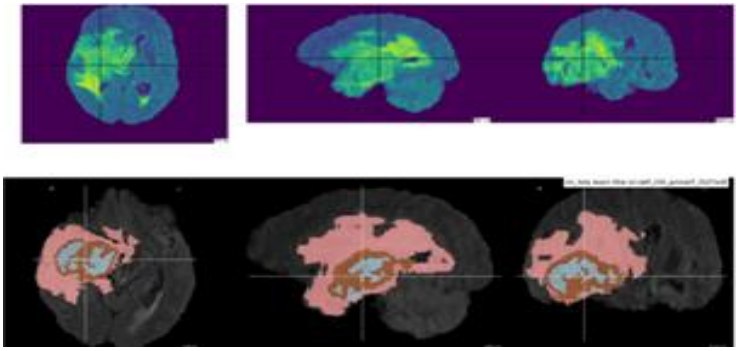

Figure 5. Various representations of the brain scan (spatial location and boundaries of the tumor)

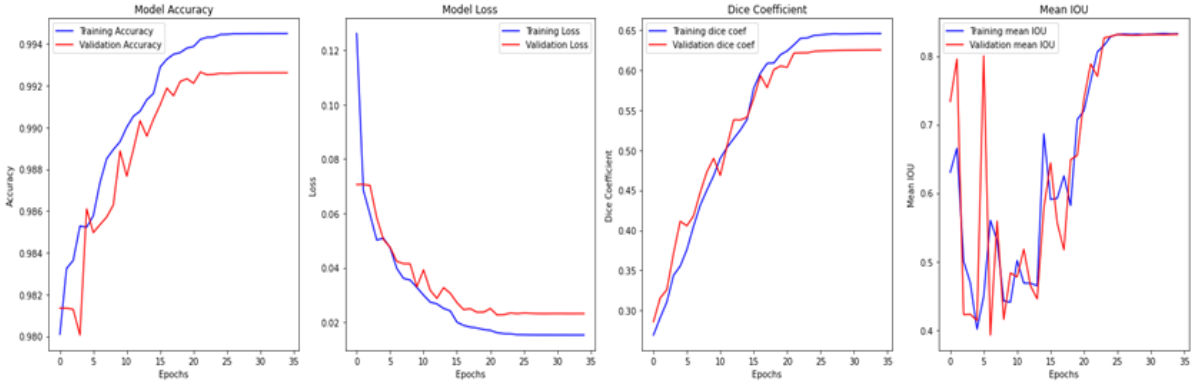

Figure 6. Training and validation metrics for tumor segmentation model

In the case below, the code imports MRI scans, ground truth segmentation masks, and model predictions, displaying them in a six images subplot, and it may utilize showPredictsById for patient comparisons as shown in Figure 7. This plot contains two subplots: The left one shows the resized ground truth for the specified class and slice, the right subplot displays the predicted segmentation for the same class and slice (in this case the 40th slice and the evaluation class are set to 2 (CORE region of the tumor), in Figure 8.

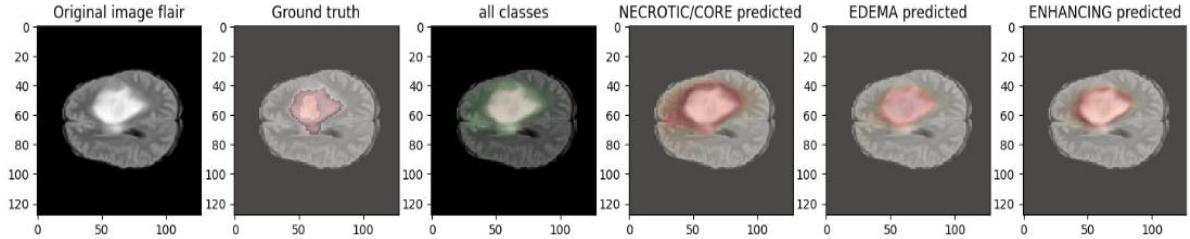

Figure 7. Tumor segmentation in MRI: original scan, ground truth, and predicted subregions for edema, core, and enhancing tumor regions (matrix size: 120×120)

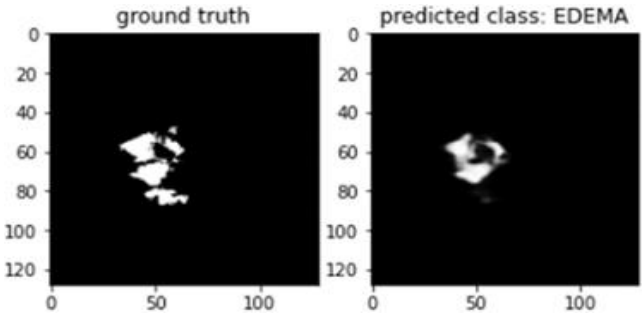

Figure 8. Subplots identify the ground truth and the predicted class (matrix size: 120x120)

6. SIMULATION RESULTS

The 3D U-Net++ model achieves superior segmentation accuracy, with a particularly low loss value (0.0146) compared to standard U-Net and Deep-Medic [3], [32], high precision (0.9951) and MeanIoU (0.8286), indicating reliable voxel categorization and remarkable overlap with background segmentations. Its Dice coefficient of 0.6452 combined with high accuracy (0.9951) and specificity (0.9984), reflects efficient and clinically reliable segmentation, particularly for regions of necrotic heart and edema. In addition, the model's high sensitivity (0.9937) underlines its effectiveness in detecting tumor cases. Dice scores for subregions confirm that 3D U-Net++ outperforms other models in feature extraction and boundary delineation in Table 2.

Table 2. Comparative performance metrics of three-dimensional segmentation models for medical imaging

Prototype	Conventional U-Net [18], [26]	Prototype	Conventional U-Net [18], [26]	Prototype	Conventional U-Net [18], [26]
Loss	0.0254	0.0196	0.0223	0.0181	0.0146
Accuracy	0.9875	0.9912	0.9890	0.9928	0.9951
MeanIoU	0.7852	0.8083	0.7920	0.8189	0.8286
Dice coefficient	0.6052	0.6238	0.6165	0.6457	0.6452
Precision	0.9831	0.9885	0.9859	0.9907	0.9953
Sensitivity	0.9784	0.9843	0.9821	0.9873	0.9937
Specificity	0.9954	0.9967	0.9959	0.9972	0.9984
Dice (necrotic core)	0.6204	0.6453	0.6309	0.6583	0.6573
Dice (edema)	0.7051	0.7321	0.7218	0.7480	0.7502
Dice (enhancing core)	0.6902	0.7105	0.7004	0.7256	0.7341

7. DISCUSSION

The 3D U-Net++ model demonstrates superior performance in automated brain tumor segmentation, consistently outperforming other models across key metrics such as loss, accuracy, Mean Intersection over Union (MeanIoU), precision, sensitivity, and specificity. It achieved the lowest loss (0.0146) and the highest accuracy (0.9951), indicating remarkable reliability in segmenting brain tumors. The MeanIoU score of 0.8286 highlights its proficiency in accurately delineating tumor boundaries, which is essential for effective surgical planning. Dice coefficients for critical tumor subregions, 0.6573 for the necrotic core, 0.7502 for edema, and 0.7341 for the enhancing core, further demonstrate the model's ability to identify and segment clinically relevant areas. High sensitivity (0.9937) ensures that tumor regions are correctly identified, minimizing residual tumor risk, while high specificity (0.9984) reduces false positives, preserving healthy tissue. These results have significant implications for surgical planning and patient safety. The model's enhanced accuracy enables neurosurgeons to make more informed decisions, maximizing tumor resection while minimizing damage to healthy brain structures-an especially critical factor in complex cases near vital brain regions. Automation of the segmentation process also alleviates clinicians' workload, allowing faster and more efficient surgical planning, which can lead to improved patient outcomes through timely interventions. From a patient safety perspective, the model's high sensitivity and specificity help reduce surgical complications and the risk of neurological deficits by preventing inadvertent removal of healthy tissue. Overall, 3D U-Net++ supports personalized, high-quality care by enabling precise and reliable tumor delineation tailored to each patient's unique anatomy.

8. CONCLUSION

The automated segmentation of glioma subregions from multimodal MRI volumes is proposed in this paper using an advanced 3D U-Net++ convolutional neural network. Four MRI sequences (T1, T1-Gd, T2, and FLAIR) are used in the procedure; these are normalized, co-registered, and resampled to improve feature extraction and guarantee data consistency. The model is trained using a composite loss function that combines Dice loss and Focal loss to address class imbalance and enhance segmentation accuracy. This allows for robust learning from both challenging and well-classified voxels. The 3D U-Net++ architecture incorporates deep supervision and dense skip connections, which enable precise delineation of complex tumor boundaries, such as necrotic core, edema, and enhancing tumor regions. The BraTS 2020 dataset is used to train and assess the model. It outperforms traditional U-Net and DeepMedic models with a remarkably low loss value (0.0146), a Dice coefficient of 0.6452, an accuracy of 0.9951, and a specificity of 0.9984. These findings show that, while preserving computational efficiency and adaptability to diverse tumor presentations, the incorporation of an optimized loss function into the 3D U-Net++ framework provides robust and dependable segmentation of glioma subregions, aids clinical decision-making in neurosurgical planning, and lessens the need for manual annotation.

9. CHALLENGES AND FUTURE WORK

Future research can benefit from enhanced training strategies that leverage consistently annotated datasets such as BraTS2021 for brain tumor segmentation and AMOS for abdominal organ delineation, which are critical for improving segmentation accuracy in complex transitional regions. Furthermore, integrating domain-adaptive training, multi-resolution inputs, and hybrid architectures with attention mechanisms may significantly refine boundary accuracy. Notably, leveraging U-Net++'s nested and dense skip connections enhances feature reusability and reduces semantic gaps between encoder and decoder, leading to superior accuracy and overlap with ground truth masks. Combining U-Net++ with powerful backbone encoders like EfficientNet can further boost performance by extracting richer multi-scale contextual features with fewer parameters, thereby improving segmentation precision, boundary sharpness, and generalization across diverse clinical datasets.

ACKNOWLEDGMENTS

This work was financially supported by the General Directorate of Scientific Research and Technological Development (DGRSDT) under the authority of the Ministry of Higher Education and Scientific Research (MESRS) and sponsored by the Laboratory of Information and Telecommunications Technologies of the Faculty of Technology, Mohammed TAHRI University-Bechar.

AUTHOR CONTRIBUTIONS STATEMENT

This journal uses the Contributor Roles Taxonomy (CRediT) to recognize individual author contributions, reduce authorship disputes, and facilitate collaboration.

Name of Author	C	M	So	Va	Fo	I	R	D	O	E	Vi	Su	P	Fu
Ahmed Bounegta	✓	✓	✓	✓	✓	✓	✓	✓	✓	✓	✓	✓	✓	✓
Mustapha Khelifi		✓		✓		✓		✓		✓			✓	
Mohammed Beladgham	✓			✓		✓	✓				✓	✓		

C : **C**onceptualization
M : **M**ethodology
So : **So**ftware
Va : **Va**lidation
Fo : **Fo**rmal analysis
I : **I**nvestigation
R : **R**esources
D : **D**ata Curation
O : Writing - **O**riginal Draft
E : Writing - Review & **E**diting
Vi : **Vi**sualization
Su : **Su**pervision
P : **P**roject administration
Fu : **Fu**nding acquisition

CONFLICT OF INTEREST STATEMENT

The authors declare that they have no known financial, personal, or professional conflicts of interest that could have influenced the work presented in this paper. All contributions were made objectively and independently.

REFERENCES

[1] B. H. Menze *et al.*, "The multimodal brain tumor image segmentation benchmark (BRATS)," *IEEE Transactions on Medical Imaging*, vol. 34, no. 10, pp. 1993–2024, Oct. 2015, doi: 10.1109/TMI.2014.2377694.

[2] S. Bakas *et al.*, "Advancing the cancer genome atlas glioma MRI collections with expert segmentation labels and radiomic features," *Scientific Data*, vol. 4, no. 1, p. 170117, Sep. 2017, doi: 10.1038/sdata.2017.117.

[3] R. A. Zeineldin, M. E. Karar, O. Burgert, and F. Mathis-Ullrich, "Multimodal CNN networks for brain tumor segmentation in MRI: a BraTS 2022 challenge solution," in *Lecture Notes in Computer Science*, vol. 13769 LNCS, 2023, pp. 127–137. doi: 10.1007/978-3-031-33842-7_11.

[4] M. Adewole *et al.*, "The brain tumor segmentation (BraTS) challenge 2023: glioma segmentation in sub-saharan Africa patient population (BraTS-Africa)," *ArXiv*. May 30, 2023. [Online]. Available: http://www.ncbi.nlm.nih.gov/pubmed/37396608%0Ahttp://www.pubmedcentral.nih.gov/articlerender.fcgi?artid=PMC10312814

[5] A. W. Moawad *et al.*, "The brain tumor segmentation (BraTS-METS) challenge 2023: brain metastasis segmentation on pre-treatment MRI." 2023. doi: 10.59275/j.melba.2025-9bd3.

[6] M. C. de Verdier *et al.*, "The 2024 brain tumor segmentation (BraTS) challenge: glioma segmentation on post-treatment MRI." 2024. [Online]. Available: http://arxiv.org/abs/2405.18368

[7] A. Crimi, L. Dodero, F. Sambataro, V. Murino, and D. Sona, "Structurally constrained effective brain connectivity," *NeuroImage*, vol. 239, p. 118288, Oct. 2021, doi: 10.1016/j.neuroimage.2021.118288.

[8] S. Bakas *et al.*, "Identifying the best machine learning algorithms for brain tumor segmentation, progression assessment, and overall survival prediction in the BRATS challenge." 2019. [Online]. Available: http://arxiv.org/abs/1811.02629

[9] S. Bauer, R. Wiest, L. P. Nolte, and M. Reyes, "A survey of MRI-based medical image analysis for brain tumor studies," *Physics in Medicine and Biology*, vol. 58, no. 13, pp. R97–R129, Jul. 2013, doi: 10.1088/0031-9155/58/13/R97.

[10] F. Isensee, P. F. Jäger, P. M. Full, P. Vollmuth, and K. H. Maier-Hein, "nnU-Net for brain tumor segmentation," *Lecture Notes in Computer Science (including subseries Lecture Notes in Artificial Intelligence and Lecture Notes in Bioinformatics)*, vol. 12659 LNCS. pp. 118–132, 2021. doi: 10.1007/978-3-030-72087-2_11.

[11] P. Li, W. Wu, L. Liu, F. Michael Serry, J. Wang, and H. Han, "Automatic brain tumor segmentation from multiparametric MRI based on cascaded 3D U-Net and 3D U-Net++," *Biomedical Signal Processing and Control*, vol. 78, p. 103979, Sep. 2022, doi: 10.1016/j.bspc.2022.103979.

[12] Y. Zhang, X. Liu, S. Wa, Y. Liu, J. Kang, and C. Lv, "GenU-Net++: an automatic intracranial brain tumors segmentation algorithm on 3D image series with high performance," *Symmetry*, vol. 13, no. 12, p. 2395, Dec. 2021, doi: 10.3390/sym13122395.

[13] Ö. Çiçek, A. Abdulkadir, S. S. Lienkamp, T. Brox, and O. Ronneberger, "3D U-net: Learning dense volumetric segmentation from sparse annotation," in *Lecture Notes in Computer Science*, vol. 9901 LNCS, 2016, pp. 424-432. doi: 10.1007/978-3-319-46723-8_49.

[14] X. Guan *et al.*, "3D AGSE-VNet: an automatic brain tumor MRI data segmentation framework," *BMC Medical Imaging*, vol. 22, no. 1, p. 6, Dec. 2022, doi: 10.1186/s12880-021-00728-8.

[15] J. Cao, J. Liu, and J. Chen, "A brain tumor segmentation method based on attention mechanism," *Scientific Reports*, vol. 15, no. 1, p. 15229, Apr. 2025, doi: 10.1038/s41598-025-98355-8.

[16] G. Litjens *et al.*, "A survey on deep learning in medical image analysis," *Medical Image Analysis*, vol. 42, pp. 60–88, Dec. 2017, doi: 10.1016/j.media.2017.07.005.

[17] F. Isensee, C. Ulrich, T. Wald, and K. H. Maier-Hein, "Extending nnU-Net is all you need." Aug. 23, 2022. [Online]. Available: http://arxiv.org/abs/2208.10791

[18] F. Isensee *et al.*, "nnU-Net Revisited: A Call for Rigorous Validation in 3D Medical Image Segmentation." Jul. 25, 2024. [Online]. Available: http://arxiv.org/abs/2404.09556

[19] D. Veiga-Canuto *et al.*, "Comparative multicentric evaluation of inter-observer variability in manual and automatic segmentation of neuroblastic tumors in magnetic resonance images," *Cancers*, vol. 14, no. 15, p. 3648, Jul. 2022, doi: 10.3390/cancers14153648.

[20] F. Isensee *et al.*, "nnU-Net: self-adapting framework for U-Net-based medical image segmentation." Sep. 27, 2018. [Online]. Available: http://arxiv.org/abs/1809.10486

[21] K. Kundal, K. V. Rao, A. Majumdar, N. Kumar, and R. Kumar, "Comprehensive benchmarking of CNN-based tumor segmentation methods using multimodal MRI data," *Computers in Biology and Medicine*, vol. 178, p. 108799, Aug. 2024, doi: 10.1016/j.compbiomed.2024.108799.

[22] N. Ayub, M. Waqas Iqbal, M. U. Saleem, M. N. Amin, O. Imran, and H. Khan, "Spectrum of engineering sciences efficient ML technique for brain tumor segmentation, and detection, based on MRI scans using convolutional neural networks (CNNs) Spectrum of Engineering Sciences," *Spectrum of Engineering Sciences*, vol. 3, no. 3, pp. 186–213, 2025.

[23] O. Ronneberger, P. Fischer, and T. Brox, "U-Net: convolutional networks for biomedical image segmentation." May 18, 2015. [Online]. Available: http://arxiv.org/abs/1505.04597

[24] K. Kamnitsas *et al.*, "Efficient multi-scale 3D CNN with fully connected CRF for accurate brain lesion segmentation," *Medical Image Analysis*, vol. 36, pp. 61–78, Feb. 2017, doi: 10.1016/j.media.2016.10.004.

[25] J. Nodirov, A. B. Abdusalomov, and T. K. Whangbo, "Attention 3D U-Net with multiple skip connections for segmentation of brain tumor images," *Sensors*, vol. 22, no. 17, p. 6501, Aug. 2022, doi: 10.3390/s22176501.

[26] K. Xu, M. Zhang, S. Jegelka, and K. Kawaguchi, "Optimization of graph neural networks: implicit acceleration by skip connections and more depth," in *International conference on machine learning*, 2021, pp. 11592–11602.

[27] B. Baheti *et al.*, "The brain tumor sequence registration (BraTS-Reg) challenge: establishing correspondence between pre-operative and follow-up MRI scans of diffuse glioma patients." Apr. 17, 2021. [Online]. Available: http://arxiv.org/abs/2112.06979

[28] J. E. H. Rivera *et al.*, "An ensemble approach for brain tumor segmentation and synthesis." Nov. 26, 2024. [Online]. Available: http://arxiv.org/abs/2411.17617

[29] F. Kofler *et al.*, "BraTS Toolkit: Translating BraTS brain tumor segmentation algorithms into clinical and scientific practice," *Frontiers in Neuroscience*, vol. 14, Apr. 2020, doi: 10.3389/fnins.2020.00125.

[30] S. Kassam, A. Markham, K. Vo, Y. Revanakara, M. Lam, and K. Zhu, "Intraoperative glioma segmentation with YOLO + SAM for improved accuracy in tumor resection." Aug. 27, 2024. [Online]. Available: http://arxiv.org/abs/2408.14847

[31] A. Ilhan, B. Sekeroglu, and R. Abiyev, "Brain tumor segmentation in MRI images using nonparametric localization and enhancement methods with U-net," *International Journal of Computer Assisted Radiology and Surgery*, vol. 17, no. 3, pp. 589–600, Mar. 2022, doi: 10.1007/s11548-022-02566-7.

[32] A. E. Orhan and X. Pitkow, "Skip connections eliminate singularities," *6th International Conference on Learning Representations, ICLR 2018 - Conference Track Proceedings*. Mar. 04, 2018. [Online]. Available: http://arxiv.org/abs/1701.09175

BIOGRAPHIES OF AUTHORS

Ahmed Bounegta was born in Algeria. He earned an engineering degree in telecommunications from the Institute of Telecommunications of Oran in Algeria in 1984, a diploma of higher technological studies from ENSEEIHT INP in Toulouse, France, in 1992, a master's degree in digital communications from TAHRI Mohamed University in Bechar, Algeria, in 2013, and a master's degree in business law from the Ministry of Commerce in 2023. He is presently a PhD candidate. He served as the Wilaya director of postal and telecommunications services and network manager during his professional career. His primary areas of study are telecommunications, networks, image processing systems, and segmentation techniques, as well as source and channel coding. He can be contacted at email: bounegta.ahmed@univ-bechar.dz.

Mustapha Khelifi He was born in Ain Sefra, Naama, Algeria. He graduated from the University DR MOULAY Tahar in Algeria with a bachelor's degree in electrical engineering in 2009, a master's degree in signal and digital communication from the University of Bechar in Algeria in 2011, and a PhD in telecommunication from the University of Bechar in Algeria in 2016. Image processing, compression, channel, and source coding are among his key interests. He can be contacted at email: khelifi.mostepha@univ-bechar.dz.

Mohammed Beladgham obtained a degree in electrical engineering and a master's in signals and systems from the University of Tlemcen in Algeria. In 2012, he earned his PhD in electronics from the University of Tlemcen in Algeria. He is presently a professor at the Department of Electrical Engineering at the Faculty of Technology, TAHRI Mohamed University of Bechar, Algeria. His research interests encompass image segmentation, medical image compression, video processing, and biomedical imaging. Presently serving as an associate director at the University of Bechar, Algeria. He can be contacted at email: beladgham.mohammed@univ-bechar.dz.